Dielectric characteristics of nanocrystalline Ag – Ba 0.5 Sr 0.5 Ti O 3 composite thin films

K. P. Jayadevan, C. Y. Liu, and T. Y. Tseng

Articles you may be interested in

Dielectric characteristics of nanocrystalline Ag−Ba$_{0.5}$Sr$_{0.5}$TiO$_3$ composite thin films

K. P. Jayadevan, C. Y. Liu, and T. Y. Tseng[a)]

Department of Electronics Engineering and Institute of Electronics, National Chiao-Tung University, Hsinchu 300, Taiwan, Republic of China

Nanocrystalline Ag−Ba$_{0.5}$Sr$_{0.5}$TiO$_3$ (Ag–BST) composite thin films are deposited on Pt/Ti/SiO$_2$/Si substrates by a sol-gel method. The voltage-dependent capacitance (C–V) and dielectric loss of the films decrease with increasing Ag up to 2 mol % due to a series configuration involving low dielectric interface layers and dense microstructures. The evidence for asymmetric distribution of charge carriers in the Ag–BST film is derived from C–V measurements. The dielectric tunability of BST film with 1 mol % Ag is comparable to that of pure BST. © *2004 American Institute of Physics*. [DOI: 10.1063/1.1780596]

There had been interest in the past several decades to discover the versatile nature of silver (Ag) in modifying the microstructure and resultant physical properties such as dielectric characteristics of insulators[1,2] and superconductivity of cuprates,[3] and recently, optical nonlinearity of Ag-dielectric composites.[4] Despite the sustained focus on the Ag-dielectric composites, there is lack of adequate consistency on how Ag affects the resultant dielectric properties of bulk Ag−BaTiO$_3$ (BTO) (Refs. 5–7) and thin films of Ag–BTO (Ref. 8) and Ag−(Ba,Sr)TiO$_3$ (BST).[9] The sol-gel-derived Ag–BTO nanocomposite thin films[8] showed a decrease in dielectric constant due to a reduction in net polarization of Ag–BTO and an increase in loss with increasing Ag up to 5 mol %. In contrast, the pulsed-laser-deposited (PLD) Ag-BST thin films[9] exhibited higher capacitance for 5 wt. % Ag-doped samples, which was ascribed to the improved oxygenation of the BST film, as metastable silver oxide phases decomposed during the thermal processing of the film and filled the oxygen vacancies. However, no dielectric loss characteristics were discussed.[9] In this letter, we report the effect of Ag addition on the capacitance and loss characteristics of sol-gel-derived Ba$_{0.5}$Sr$_{0.5}$TiO$_3$ thin films. Ba$_{0.5}$Sr$_{0.5}$TiO$_3$, which is a high permittivity, low loss paraelectric material suitable for integrated capacitor applications,[10] in combination with small amounts of Ag would form a potential metal-dielectric composite for electromagnetic wave propagation.

The pure Ba$_{0.5}$Sr$_{0.5}$TiO$_3$ (BST) and (1 mol % and 2 mol %) Ag–(99 mol % and 98 mol %) Ba$_{0.5}$Sr$_{0.5}$TiO$_3$ (Ag(1)–BST and Ag(2)–BST) thin films were prepared by an acetate precursor sol-gel route.[11] Stoichiometric amounts of the starting materials, Ba(OAc)$_2$, Sr(OAc)$_2$, Ag(OAc), and Ti(i-OPr)$_4$ (OAc-Acetate, i-OPr-Isopropoxide), were dissolved in acetic acid and ethylene glycol (3:1) and stirred at 90 °C for about 60 min. The above prepared 0.15 M precursor solutions were spin-coated on Pt(100 nm)/Ti(5 nm)/SiO$_2$ (500 nm)/Si substrates in two steps (1000 rpm for 15 s and 4000 rpm for 60 s) in order to achieve a uniform coating. Each deposited layer was heat-treated at 200 °C for 10 min and then 500 °C for 30 min. The coating and pyrolysis steps were repeated to obtain the desired film thickness. The films were finally annealed at

700 °C for 2 h in air and characterized for phase formation and grain size using x-ray diffraction (XRD, Cu $K\alpha$, λ =0.15405 nm, 0.02° 2θ step, Rigaku DMaxB x-ray diffractometer), and microstructure using scanning electron microscopy (SEM, Hitachi S4700). For dielectric characterization, metal-insulator-metal (MIM) structures were fabricated by depositing 100 nm thick Pt top electrodes with a diameter of 250 μm by electron beam evaporation through a shadow mask. The capacitance–voltage (C–V) and dielectric loss characteristics were measured using HP4284A LCR Meter from −6 to +6 V and back with a step voltage of 0.1 V at 100 kHz.

Figure 1 shows the XRD patterns of BST, Ag(1)–BST, and Ag(2)–BST films. All the diffraction peaks are indexed to BST phase with (200) being the most intense peak in all the three samples. As silver oxides are unstable[12] at the annealing temperature (700 °C), the presence of any oxide phases of silver is ruled out in the Ag-BST films. The diffraction peaks of Ag(1)–BST and Ag(2)–BST do not show any shifts with reference to those of pure BST when recorded for three sets of samples, indicating negligible solubility of
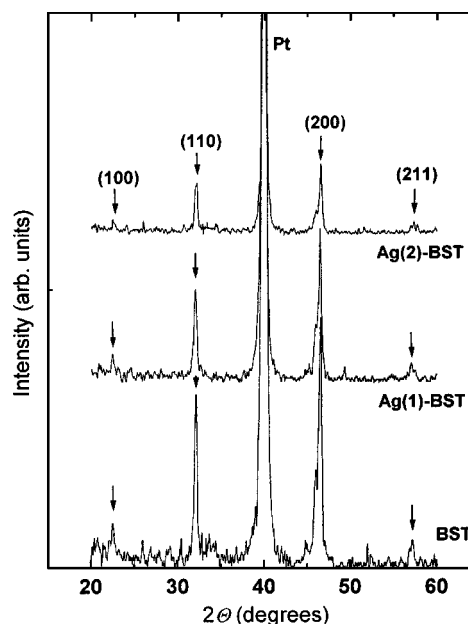

FIG. 1. XRD patterns of BST, Ag(1)–BST, and Ag(2)–BST thin films.

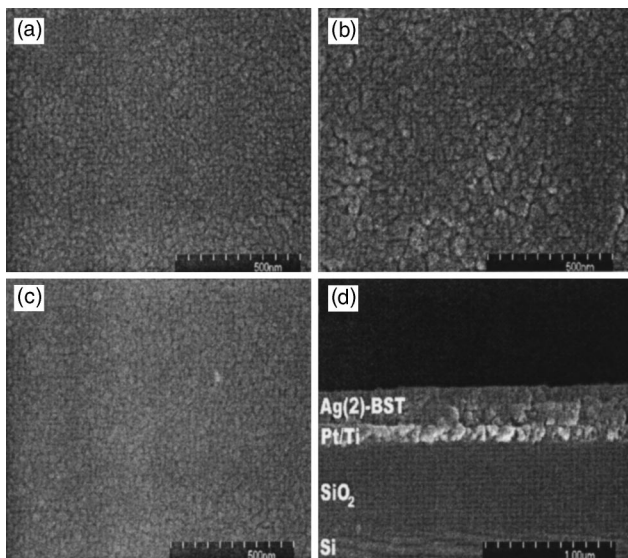[a)]Electronic mail: tseng@cc.nctu.edu.tw

FIG. 2. SEM pictures of surface morphologies of sol-gel-derived (a) BST, (b) Ag(1)–BST, (c) Ag(2)–BST thin films, and (d) cross-sectional SEM picture of Ag(2)–BST film (thickness $\sim 210 \pm 10$ nm) on Pt/Ti/SiO$_2$/Si substrates indicating dense microstructure.

FIG. 3. $C–V$ characteristics of BST, Ag(1)–BST, and Ag(2)–BST films measured in the range $-6 \leftrightarrow +6$ V.

Ag in BST. The gradual reduction in intensities of diffraction peaks for Ag(1)–BST and Ag(2)–BST could have been caused by an increase in the degree of disorder in the orientation of the crystallites induced by the modification of grain boundary atomic configuration by Ag.[9] The full-width at half maxima (FWHM, β) of (110) and (200) peaks and the average grain sizes ($t_{XRD} = 21 \pm 2$ nm) obtained by Scherrer equation at corresponding Bragg angles, θ_B, ($t_{XRD} = 0.9\lambda/\beta \cos \theta_B$, where λ is the wavelength of the Cu $K\alpha$ radiation) remain unchanged, as the amounts of Ag added are insufficient to form an enough second phase and affect these parameters.

Figure 2 depicts the SEM analysis of the surface morphologies of BST, Ag(1)–BST and Ag(2)–BST films and cross section for the Ag(2)–BST film. For pure BST, the SEM study reveals fairly uniform agglomerates with average diameter (d_{SEM}) of ~ 27 nm [Fig. 2(a)]. An increase in nonuniformity is observed for the d_{SEM} of Ag(1)–BST film with an average value of ~ 40 nm [Fig. 2(b)] that differs much from the primary particle or grain size obtained by XRD t_{XRD}. The presence of nonuniform agglomerates on the surface of the Ag(1)–BST film has been found to be reproducible upon the SEM examination of surface morphology of four samples. The formation of large and dense Ag(1)–BST agglomerates could be due to the enhanced grain boundary diffusion caused by the space charge effect across the Ag/BST interfaces as a result of Fermi energy equalization upon the addition of a small and critical amount of Ag.[5–7] For the Ag(2)–BST film, the agglomerate size ($d_{SEM} \sim 25$ nm) is highly uniform with no large ones observed. The microstructure is better than pure BST and Ag(1)–BST with considerable reduction in porosity [Fig. 2(c)], which could be due to the low solubility of Ag in BST grains and its increased presence along the grain boundaries.[9] The cross-sectional SEM analysis [not shown here for BST and Ag(1)–BST] indicates that the 210 ± 10 nm thick films on Pt/Ti/SiO$_2$/Si have clearly distinguishable, crack-free interfaces. The dense microstructure of Ag(2)–BST is further demonstrated by a cross-sectional SEM picture as shown in Fig. 2(d).
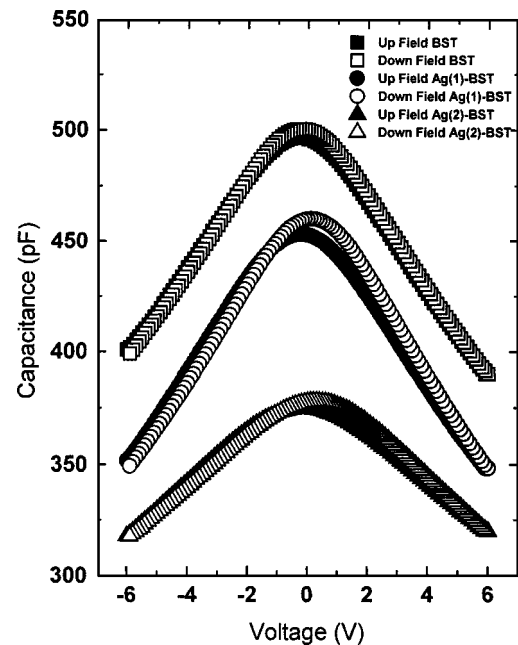
The $C–V$ characteristics for pure BST, Ag(1)–BST, and Ag(2)–BST films in the range from -6 to $+6$ V are presented in Fig. 3. The $C–V$ curve for pure BST under increasing and decreasing field has identical position for maximum effective capacitance (C_m). No broadening of the $C–V$ curve is observed for Ag(1)–BST despite a reduction in capacitance relative to pure BST and a slight positive shift ($\sim +0.1$ V) of the C_m in the down field. For the Ag(2)–BST film, the $C–V$ curve broadens and is associated with lowering and shifting of the C_m to $\sim +0.2$ V in the down field. These observations can be explained as follows: As obtained from the SEM analysis, the BST and Ag–BST have typical microstructures that are reminiscent of films prepared by solution deposition route with randomly oriented nanocrystalline grains aligned parallel to the substrate. Therefore, the effective capacitance (C_{eff}), which comprises the contributions from the grain interior of the film (C_{gf}), film/electrode interface (C_i), and grain boundary (C_{gb}), can be expressed in a series capacitor configuration[13] as,

$$1/C_{eff} = 1/C_{gf} + 1/C_i + 1/C_{gb}. \tag{1}$$

Of the three terms, the reduction in C_{eff} of the Ag(1)–BST and Ag(2)–BST films could have been caused by the low C_{gb}, since Ag has limited solubility in the BST lattice and is expected to modify the grain boundary atomic configuration.[9] In a nanocrystalline sample, C_{gb} is predominant. The formation of a film/electrode interfacial layer with a low C_i cannot be ruled out as Ag might diffuse to the interface. The consequences of such grain boundary modification or low dielectric interface formation are a reduction in C_{eff} and a slight shift in the $C–V$ maxima of Ag(1)–BST and Ag(2)–BST films when measured down field indicative of an asymmetric distribution of the charge carriers in the film. The product $C_m \times \Delta V$ is a measure of the accumulated charge where C_m is the maximum effective capacitance and ΔV is the corresponding voltage shift.[13] That the ΔV is greater for Ag(2)–BST implies an increase in charge accumulation with increasing Ag in BST. The positive $C–V$
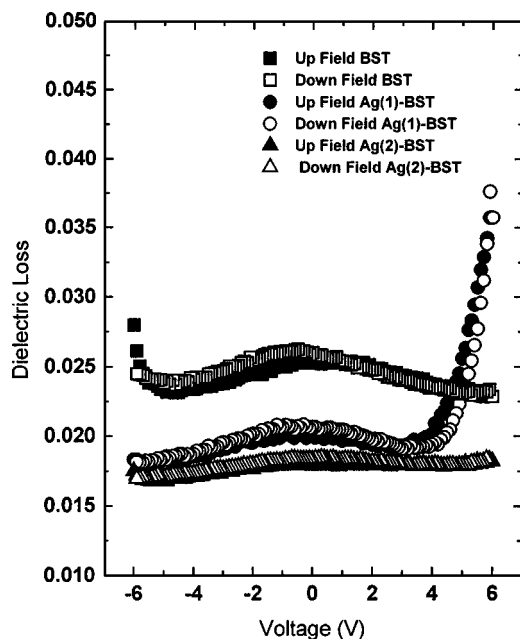
FIG. 4. Dielectric loss (tan δ) characteristics of BST, Ag(1)–BST, and Ag(2)–BST measured in the range $-6 \leftrightarrow +6$ V.

shifts[14] for Ag(1)–BST and Ag(2)–BST upon reversing the field indicate the presence of excess negatively charged species (electrons from Ag) near to the top electrode, which also indirectly points to the direction of diffusion of the Ag as towards the surface of the film, thereby modifying the top electrode/film interface. The identical position of C_m for pure BST in either sweeps confirms the absence of accumulated charge.

It is interesting to note that the tunability ($=C_0-C_V/C_0$, where C_0 and C_V are the capacitance at zero and maximum bias voltages) of the C–V curve for Ag(1)–BST film ($22\pm2\%$) is comparable or marginally higher than pure BST ($21\pm2\%$). Improvement in dielectric tunability is often associated with better crystallinity of the film. In this case, on the contrary, we observe a reduction in intensity of the diffraction peaks as shown by XRD, without lowering of tunability. This observation may be correlated to the typical microstructure, which shows that the 1 mol % Ag addition improves the densification of the BST nanograins forming large agglomerates [Fig. 2(b)]. The large agglomerates may have grains with identical polarization behavior causing an increase in polarization density, which results in the observed dielectric tunability being equal or marginally better than pure BST. The significant broadening of the capacitance with a reduction in tunability ($15\pm2\%$) for Ag(2)–BST film is due to the inability of the dipole moments in the BST nanograins to orient in the presence of applied field because of the enhanced pinning effect of Ag (Ref. 9) along the grain boundaries, as the SEM picture [Fig. 2(c)] reveals the absence of large agglomerates of Ag(2)–BST unlike that of the Ag(1)–BST film [Fig. 2(b)]. The average dielectric constants for the C_m of BST, Ag(1)–BST and Ag(2)–BST correspond to 237, 222, and 182, respectively with $\sim\pm10$ variation.

Figure 4 shows the dielectric loss (tan δ) of pure BST, Ag(1)–BST, and Ag(2)–BST films. At zero bias voltage,

tan δ decreases in the order of BST (0.025) $>$ Ag(1)–BST (0.02) $>$ Ag(2)–BST (0.018) with $\sim\pm0.001$ variation. For the entire range of measurement ($-6 \leftrightarrow +6$ V or $-286 \leftrightarrow +286$ kV/cm), the tan δ of Ag(2)–BST is the lowest. The dense microstructure of Ag(2)–BST is one of the reasons for the lowest loss. As the nonagglomerated nanocrystalline Ag(2)–BST grains have more grain boundaries [Fig. 2(c)], and relaxational loss from the grain boundaries is negligible,[15] a reduction in loss characteristics is expected. Moreover, the presence of small amounts of Ag along grain boundaries or interfaces enhances the polarization pinning,[9] and lowers the effective resistance (R) and hence tan δ ($=\omega RC$, where ω is the frequency and C the capacitance) for a series metal-ceramic configuration[5] of Ag and BST, which lead to low effective dielectric loss. The sharp increase in loss for Ag(1)–BST beyond $+4$ V may be due to the typical microstructure, which has nonuniform agglomerates that leads to variation in local electric field at high enough applied potential. From the tunability and tan δ at zero bias, the figure of merit (FOM$=$tunability/tan δ) of the three films can be estimated. The highest FOM ($=11$) is obtained for the Ag(1)–BST film.

In conclusion, the dielectric characterization of sol-gel-derived nanocrystalline Ag–Ba$_{0.5}$Sr$_{0.5}$TiO$_3$ (BST) composite films indicates that the capacitance and dielectric loss (tan δ) decrease with increasing Ag up to 2 mol % based on a series configuration involving low dielectric interface layers. The dielectric tunability of 1 mol % Ag–BST is marginally better than pure BST. The 2 mol % Ag–BST has the lowest tan δ at zero bias, which is preserved in the entire sweeping cycle because of its dense microstructure, low relaxational loss, and enhanced polarization pinning along the grain boundaries.

[1]H. Ikushima and S. Hayakawa, Jpn. J. Appl. Phys. **4**, 328 (1965).
[2]G. H. Maher, J. Am. Ceram. Soc. **66**, 408 (1983).
[3]H. S. Koo, W.-M. Hurng, W. H. Lee, T. Y. Tseng, M. Chen, and R. Lo, Appl. Phys. Lett. **62**, 3354 (1993).
[4]Q. F. Zhang, W. M. Liu, Z. Q. Xue, J. L. Wu, S. F. Wang, D. L. Wang, and Q. H. Gong, Appl. Phys. Lett. **82**, 958 (2003).
[5]N. Halder, A. D. Sharma, S. K. Khan, A. Sen, and H. S. Maiti, Mater. Res. Bull. **34**, 544 (1999).
[6]C.-Y. Chen and W.-H. Tuan, J. Am. Ceram. Soc. **83**, 2988 (2000).
[7]R. Z. Chen, X. Wang, Z. L. Gui, and L. T. Li, J. Am. Ceram. Soc. **86**, 1022 (2003).
[8]J. Zhou, L. T. Li, Z. Gui, X. Zhang, and D. J. Barber, Nanostruct. Mater. **8**, 321 (1997).
[9]A. Srivastava, D. Kumar, R. K. Singh, H. Venkataraman, and W. R. Eisenstadt, Phys. Rev. B **61**, 7305 (2000).
[10]M. S. Tsai, S. C. Sun, and T. Y. Tseng, J. Appl. Phys. **82**, 3482 (1997).
[11]D. M. Tahan, A. Safari, and L. C. Klein, J. Am. Ceram. Soc. **79**, 1593 (1996).
[12]J. Assal, B. Hallstedt, and L. J. Gauckler, J. Am. Ceram. Soc. **80**, 3054 (1997).
[13]S. Saha and S. B. Krupanidhi, J. Appl. Phys. **87**, 3056 (2000).
[14]R.-V. Wang, R. J. Becker, and P. C. McIntyre, J. Electroceram. **9**, 25 (2002).
[15]T. M. Shaw, S. T. McKinstry, and P. C. McIntyre, Annu. Rev. Mater. Sci. **30**, 263 (2000).